Thin Films of Single-Crystalline SrTiO3 Nanorod Arrays and Their Surface Wettability Conversion

ARTICLE *in* THE JOURNAL OF PHYSICAL CHEMISTRY C · AUGUST 2007

Impact Factor: 4.77 · DOI: 10.1021/jp073604z

1 AUTHOR:

Masahiro Miyauchi
Tokyo Institute of Technology
96 PUBLICATIONS **3,545** CITATIONS

Thin Films of Single-Crystalline $SrTiO_3$ Nanorod Arrays and Their Surface Wettability Conversion

Masahiro Miyauchi[†]

Nanotechnology Research Institute, National Institute of Advanced Industrial Science and Technology (AIST), Tsukuba Central 5, 1-1-1 Higashi, Tsukuba, Ibaraki 305-8565, Japan

Received: May 11, 2007; In Final Form: June 21, 2007

Thin films of single-crystalline $SrTiO_3$ nanorod arrays were synthesized by ion-exchange and annealing titanate nanotube arrays. The diameter of the $SrTiO_3$ nanorods ranged from 10 to 20 nm, and the long length axis of these nanorods was oriented in the [110] direction of the perovskite phase. These nanorod arrays were optically semitransparent and adhered well to the substrates. Due to their surface nanostructures, these nanorod surfaces exhibited superhydrophilicities with water contact angles (θ) below 3°. In addition, these surfaces turned into high-hydrophobic states ($\theta = 140°$) when oleic acid was applied. UV illumination caused these hydrophobic thin films to become superhydrophilic states because single-crystalline $SrTiO_3$ nanorods have strong photocatalytic oxidative activities, which decomposed the surface-adsorbed oleic acid.

Introduction

Strontium titanate ($SrTiO_3$) with a perovskite structure is known for its unique dielectric, thermoelectricity,[1] magnetoresistivity,[2] high-K dielectric,[3] and optical nonlinearity.[4] Besides these electronic and optical properties, $SrTiO_3$ is also known as an efficient photocatalyst for the production of gaseous hydrogen from water and for the decomposition of various organic compounds.[5] The crystal phase of $SrTiO_3$ is perovskite-type (ABO_3); thus, the charge balance is easily controllable under carrier-doping process. Recently, codoped $SrTiO_3$ such as $Sb^{5+}-Cr^{3+}$,[6] $Ag^{+}-Pb^{2+}$,[7] or $N^{3-}-La^{3+}$ doped $SrTiO_3$[8] has been reported as a highly active photocatalyst. On the other hand, one-dimensional (1-D) nanostructural control is expected to improve the performance of the electronic or photochemical properties, and single-crystalline perovskite nanorods grown by the pulsed laser ablation method have been reported.[9] In contrast, wet chemical processes have attracted much attention due to their mass-production capabilities, and nanotubes or nanorods of perovskite-type metal oxides have been synthesized via a chemical route.[10] Recently, Mao et al. have reported the hydrothermal synthesis of strontium titanate nanotubes using a titanate nanotube as a precursor, i.e., a mixture of titanate nanotubes and strontium ions in an aqueous solution was refluxed to produce $SrTiO_3$ nanotubes.[11] On the other hand, the thin film form of highly ordered single-crystalline 1-D $SrTiO_3$ arrays via a chemical route has yet to be reported. Thin film fabrication is a key technology for device applications such as semiconductors, light emitting diodes, photovoltaics, catalysis, and sensors. In particular, high crystallinity and 1-D nanostructural control of thin films are essential factors for high performance in thin film based devices.

In the present paper, single-crystalline $SrTiO_3$ nanorod arrays were successfully fabricated by ion-exchange and annealing titanate nanotube arrays. Their surface wettability behaviors were evaluated. Although my previous study revealed that polycrystalline $SrTiO_3$ does not become a superhydrophilic state with a water contact angle below 5°,[12] single-crystalline nanorod arrays in the present study have strong photocatalytic oxidative activities and do become superhydrophilic states with band gap excitation. The generation of superhydrophilicity on the $SrTiO_3$ nanorod arrays is attributed to the surface nanostructures. In the present study, the relationship between the morphology and the surface wettability behavior of $SrTiO_3$ nanorod arrays is discussed.

Experimental Section

Single-crystalline $SrTiO_3$ nanorod arrays were synthesized by ion-exchange and subsequent annealing of titanate nanotube arrays. First, the titanate nanotube arrays were synthesized by a hydrothermal treatment of titanium films on sapphire substrates.[13] Polycrystalline titanium films were deposited on sapphire substrates by rf magnetron sputtering. Sputtering was conducted under an argon gas pressure of 0.5 Pa for 20 min at room temperature with an rf power of 200 W. The Ti films were 200 nm thick. To grow the titanate nanotube arrays, these Ti films were immersed into 10 M aqueous NaOH solution and heated at 393 K for 2 h in a PTFE-lined autoclave. Then these films were washed with pure water and immersed in 0.1 M HNO_3 aqueous solution for 1 h to protonate the surfaces of the titanate nanotubes. Afterward, they were immersed in a saturated strontium acetate solution (2.0 M in aqueous solution) for 15 h at room temperature to exchange the protons with strontium ions (Sr^{2+}) in the interlayer of the titanate nanotubes. After drying, the samples were annealed at 823 or 923 K for 1 h in air and were subsequently washed with 0.1 M HNO_3 aqueous solution and pure water to extract strontium carbonate.

The crystal phases of the thin films were evaluated by the grazing angle method of X-ray diffraction with Cu K α rays (XRD model RINT-2100, Rigaku Co., Tokyo, Japan). The incident angle was fixed at 0.5°, while 2θ was scanned in the range of 5−70°. The morphologies of these films were observed using a scanning electron microscope (SEM model S-4800, Hitachi Co., Tokyo, Japan) and a transmission electron microscope (TEM model H-9000UHR, Hitachi, Co., Tokyo, Japan). The surface morphologies were also observed by an atomic force microscope (AFM, Nanoscope 3a, Digital Instruments). AFM

[†] Fax: +81-29-861-6299. E-mail: m-miyauchi@aist.go.jp.

10.1021/jp073604z CCC: $37.00
Published on Web 08/02/2007

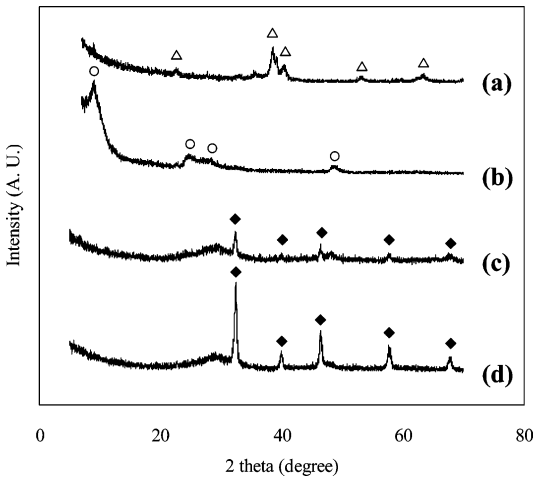

Figure 1. XRD patterns for thin films analyzed by the grazing angle method: (a) metal titanium film; (b) titanate nanotube; (c and d) annealing titanate nanotube at 823 and 923 K, respectively. Crystal phases: open triangles, titanium; open circle, titanate; closed diamond, perovskite $SrTiO_3$.

measurements were performed in the tapping mode using silicon tips. The roughness factors (*r*) were calculated by image processing of the AFM images where *r* is defined as the ratio of the actual area of a rough surface to the geometric projected area. The contact angle was measured at room temperature (295 K) using a commercial contact angle meter (CA-X, Kyowa Interface Science, Saitama, Japan) with an experimental error of $\pm 1°$ by the sessile drop method. This contact angle meter was equipped with a light source to capture water droplet images using a CCD camera. This light source did not contain UV light and, thus, did not excite the $SrTiO_3$ films. The contact angle was determined by numerically drawing a tangent close to the edge of the droplet. All measurements were performed with high-purity water. Thin films were stored in the dark under clean air (N_2/O_2 = 80/20% gas mixture) to avoid adsorption of contaminants in the air. The water contact angles of the thin films were measured under clean dark conditions. In addition, oleic acid was applied to the surfaces of these films, and the changes in the water contact angles were measured under UV illumination. Oleic acid was dissolved in ethanol with a concentration of 2.0 wt %, and this solution was coated on $SrTiO_3$ films by spin coating at a speed of 2000 rpm. UV illumination was provided by a 10 W black light bulb (Toshiba Co., Tokyo, Japan) with a light intensity of 2.0 mW/cm^2 as measured by a UV radiometer (UVR-2, Topcon Co. Tokyo, Japan). X-ray photoelectron spectroscopy (XPS) with Al Kα X-rays (model Quantum 2000, Physical Electronics) evaluated the amount atomic carbon on thin films. The photoelectrons of the Sr(3d), Ti(2p), and C(1s) orbitals were recorded with a takeoff angle of 45°. The integrated peak areas of each orbital were calculated after subtracting the nonlinear background. Quantitative analysis was based on the peak area multiplied by sensitivity factors supplied by Physical Electronics, which accounted for the geometric configuration of the apparatus.

Results and Discussion

Figure 1 shows the XRD patterns for the thin films. A hydrothermal reaction converted the polycrystalline metal titanium phase to the titanate structure. Several groups have reported that the unit cell structures of hydrothermally grown titanate nanotubes are trititanate ($H_2Ti_3O_7$),[14] lepidocrocite ($H_xTi_{2-x/4}[\ ]_{x/4}O_4$, $x \sim 0.7$, [ ] = vacancy),[15] $H_2Ti_2O_4(OH)_2$,[16] or $H_2Ti_4O_9$.[17] These reports indicate that the crystal structure is hydrogen titanate, which is composed of scrolled TiO_2 sheets that are separated by H^+ ions. The XRD pattern of the hydrothermally treated thin film in the present study is identical to the previous reports, indicating that the crystal structure of this film is hydrogen titanate. The diffraction peak observed near 9.0° corresponds to the interlayer separation between the TiO_2 sheets with a separation of 0.98 nm. On the other hand, it is noteworthy that the titanate phase is converted into a single phase of perovskite $SrTiO_3$, when titanate films are immersed in a saturated aqueous solution of strontium acetate and annealed in air. Annealing at a higher temperature causes a higher crystallinity of $SrTiO_3$ films. When the titanate thin films are annealed in air without immersion in an aqueous strontium acetate solution, the crystal structure changes from titanate to anatase TiO_2.[13a] Because titanate nanotubes are composed of scrolled TiO_2 sheets, cations such as H^+ or NH_4^+ ions can easily diffuse into the interlayer of the TiO_2 sheets.[18] Sun and Li have reported that titanate nanotubes are ion-exchangeable, and cobalt ions-substituted titanate nanotubes are transformed into a mixture of $CoTiO_3$ and rutile TiO_2 by annealing in air at 1123 K.[19] The ion radius of the 12 coordinated strontium ions (Sr^{2+}) is 0.144 nm, which is smaller than the interlayer separation between the TiO_2 sheets of titanate nanotubes (0.98 nm). The surfaces of titanate nanotubes are negatively charged[20] and have good affinities to cations. Therefore, strontium ions (Sr^{2+}) are easily diffused into the interlayer of scrolled titanate nanotubes, and protons at the interlayer can be exchanged by strontium ions. Annealing Sr^{2+}-exchanged titanate nanotubes causes a crystal transformation into the perovskite phase of $SrTiO_3$. It should be emphasized that the surface protonation procedure on titanate nanotubes before immersion into the saturated strontium acetate solution is very important for growing single-crystalline $SrTiO_3$ nanorods because the remaining sodium ions (Na^+) at the interlayer of the nanotubes suppress crystal growth of $SrTiO_3$. Hereafter, "STO-823K" and "STO-923K" refer to the $SrTiO_3$ films annealed at 823 and 923 K, respectively.

Figure 2 shows the cross-sectional SEM images of STO-823K and STO-923K films. Both films exhibit fibrous structures grown to the substrates. These films are about 600−700 nm thick, but the metal titanium film is 200 nm thick. The formation of titanate nanotubes from metal titanium under hydrothermal conditions has previously been reported,[21] whereas hydrothermal treatment has been reported to cause the dissolution of metal titanium and the nuclei for subsequent growth of the crystalline titanate nanotubes.[13a] Although cracks are seen at the interface between the substrate and nanorods, these cracks are formed during a substrate breaking procedure for measuring the cross-sectional images. The as-prepared thin films of $SrTiO_3$ are well adhered to the substrates. Figure 3 shows the SEM and AFM images for the surfaces of the thin films. Both STO-823K and STO-923K films exhibit rough surfaces with porous structures. The roughness factors (*r*), which is defined as the ratio of the actual area of a rough surface to the geometric projected area, for STO-823K and STO-923K are 2.5 and 2.6, respectively.

To investigate the crystal structure of $SrTiO_3$ nanorods more definitively, TEM analysis was performed on several nanorods grown on a STO-923K film. Figure 4 shows images for two nanorods. The diameters of these $SrTiO_3$ nanorods are 10−20 nm. Lattice fringes are observed in the high-resolution TEM (HR-TEM) images, but grain boundaries were not observed, indicating that these nanorods are single crystals. The *d* spacing estimated from the lattice fringe is 0.28 nm, which corresponds

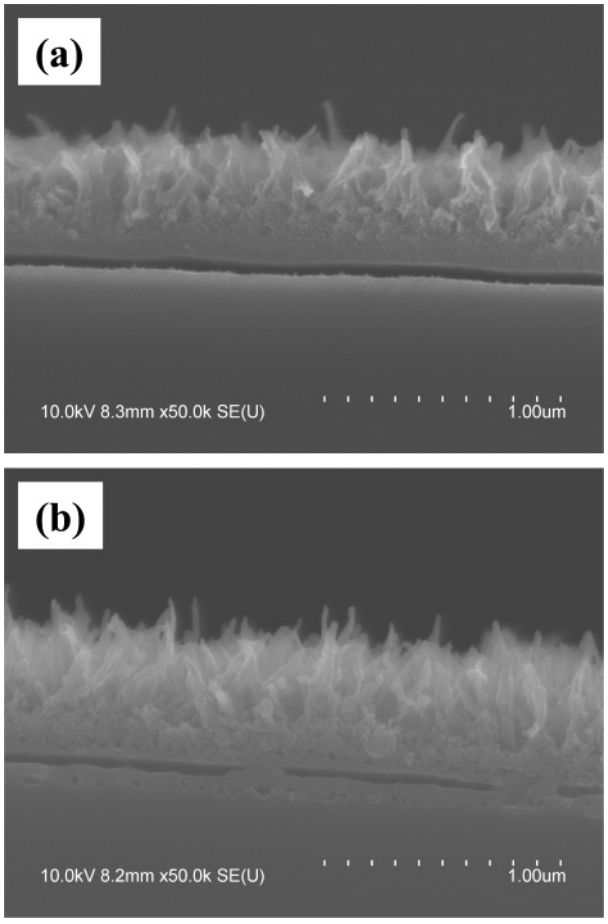

Figure 2. Cross-sectional SEM images for thin films: (a) STO-823K; (b) STO-923K.

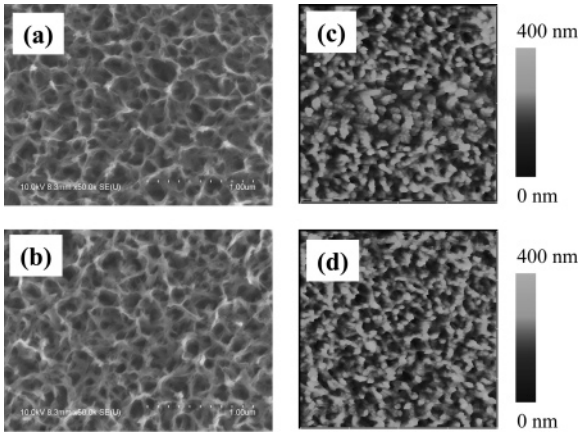

Figure 3. SEM and AFM images for the thin film surfaces: (a and b) SEM images for STO-823K and STO-923K; (c and d) AFM images for STO-823K and STO-923K, respectively.

to $SrTiO_3$ (110). The electron diffraction patterns indicate that the long axis of these nanorods is equivalent to the [110] direction. The (110) face has 12 equivalent faces, and the lattice fringes observed in both parts c and d of Figure 4 are equivalent faces of (110). Several other nanorods were observed by TEM. Consequently, similar [110] orientations are confirmed. XRD patterns (Figure 1) indicate that thin films of $SrTiO_3$ nanorods have a polycrystalline perovskite structure, since most of the nanorods are not just grown perpendicular to the substrate, and there are also polycrystalline $SrTiO_3$ grains at the interface layer

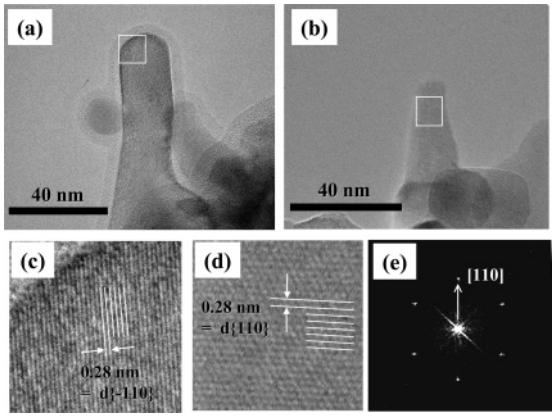

Figure 4. TEM images for STO-923K. Panels a and b are TEM images for individual nanorods. Panels c and d are the HR-TEM images for (a) and (b). Panel e is the electron diffraction pattern for image b.

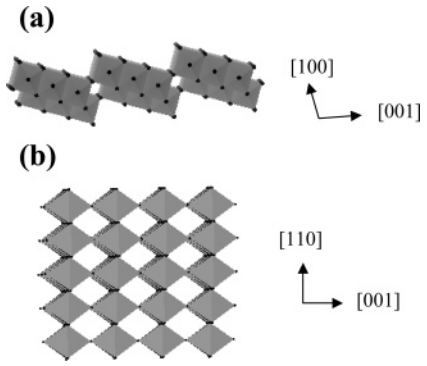

Figure 5. Crystal structures of (a) trititanate and (b) perovskite $SrTiO_3$.

between the substrate and nanorod arrays as shown in the cross-sectional SEM images (Figure 2). On the basis of TEM analysis, each $SrTiO_3$ nanorod grown on a substrate is a single crystal, whereas XRD measurements reveal that the thin films have a polycrystalline structure.

The starting materials of titanate nanotubes are thermodynamically metastable;[22] thus, a heat treatment, an acid treatment, or a hydrothermal reaction transforms the nanotubes into TiO_2 nanorods.[23,24] Figure 5a shows the crystal structure of trititanate ($H_2Ti_3O_7$). Chen et al. have reported that the titanate nanotubes are composed of layers of TiO_6 octahedrons, and the long length axis of the nanotubes is along the [010] direction.[14] Scrolled structures are constructed by wrapping the (100) plane of titanate. Gateshki et al. reported the titania nanosheet was transformed into a particular titania polymorph by rearranging the layers in a controlled way.[25] Among TiO_2 polymorphs, the rutile structure is less similar to the titania nanosheet, since it contains corner-shared TiO_6 octahedrons. Yin et al. reported that the rutile phase is not easily obtained from the titanate at mild conditions as compared to anatase or brookite phases.[26] The perovskite-type $SrTiO_3$ is constructed by corner-sheared TiO_6 octahedrons as shown in Figure 5b, and it has low lattice similarity to the titania nanosheet. The (110) structure of $SrTiO_3$ consists of O_2 and SrTiO atomic layers, and the top layer of the (110) face is terminated with O_2.[27] The common orientation relationship between [110] $SrTiO_3$ and [001] rutile TiO_2 has been observed in heteroepitaxially grown $SrTiO_3$ films, due to their lattice similarity.[28] Similar to the rutile case, a crystal transformation from titanate to perovskite is not simply explained by a dehydration and condensation process because the transformation involves a large lattice distortion. Urban et al.

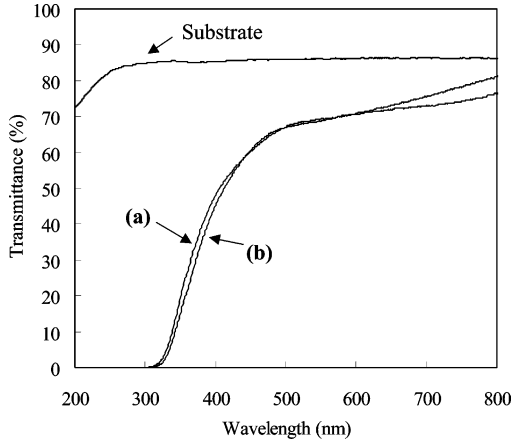

Figure 6. UV−vis spectra for thin films: (a) STO-823K and (b) STO-923K.

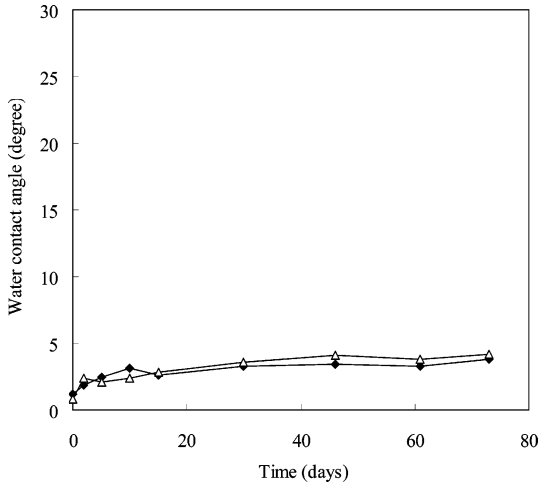

Figure 7. Change in the water contact angles under dark storage in clean air: closed diamond, STO-823K; open triangle, STO-923K.

reported that the single-crystalline perovskite nanowires were synthesized via a high-temperature hydrothermal treatment (553 K).[10a] In the present study, the annealing temperature in air must be above 723 K to form (110)-oriented $SrTiO_3$ nanorods. Under this high-temperature condition, diffusion of ions in a crystal can occur and the crystal is rearranged into a thermodynamically stable structure. The (110) face of $SrTiO_3$ is considered to be one of the most energetically stable crystal faces, similar to the (100) face.[27]

Figure 6 shows the UV−vis spectra for the thin films. The transmittance of the $SrTiO_3$ films decreases around 400 nm due to the interband transition of $SrTiO_3$. The valence and conduction bands of $SrTiO_3$ consist of O-2p orbital and Ti-3d orbital, respectively, and its band gap is about 3 eV.[29] Both STO-823K and STO-923K exhibit similar optical absorption behaviors and are semitransparent in the visible light region.

Figure 7 shows the changes in the water contact angles when the STO-823K and STO-923K films are stored in the dark in clean air conditions. The initial contact angles for both films are very low (below 3°), and these superhydrophilic states remain for more than 2 months. These superhydrophilicities of $SrTiO_3$ nanorod arrays are attributed to their surface morphologies. Wenzel has proposed a theoretical model to describe the contact angle at a rough surface (θ').[30] He modified Young's equation using the roughness factor (r) as follows:

$$\cos\theta' = r(\gamma_{SV} - \gamma_{SL})/\gamma_{LV} = r\cos\theta \qquad (1)$$

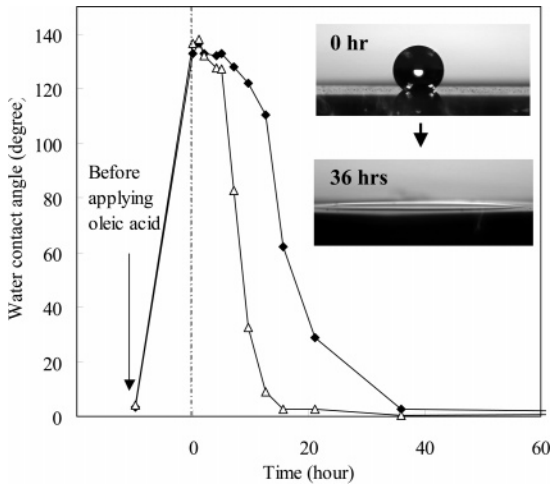

Figure 8. Time dependence of the water contact angle under UV illumination after applying oleic acid to the thin film surfaces: closed diamond, STO-823K; open triangle, STO-923K. Insets show photographs of water droplets on the surface of STO-923K before and after UV illumination.

where r is defined as the ratio of the actual area of the rough surface to the geometric projected area, and γ_{SL}, γ_{SV}, and γ_{LV} are the interfacial free energy per unit area of the solid−liquid, solid−gas, and liquid−gas interfaces, respectively. This equation indicates that surface roughness enhances the hydrophilicity of hydrophilic surfaces ($\theta < 90°$) and the hydrophobicity of hydrophobic ones ($\theta > 90°$) because r is always greater than 1. I have previously reported the surface wettability of polycrystalline $SrTiO_3$ thin films, and the initial water contact angle in the dark under clean air is 22°.[12] AFM analysis indicates that the roughness factor r of this film is 1.1. With the use of these experimental results, the estimated contact angle of a flat $SrTiO_3$ surface is 33° by Wenzel's equation. In the present paper, AFM analysis indicates that the roughness factor of STO-823K and STO-923K are 2.5 and 2.6, respectively. Considering these roughness factors and the estimated contact angle of a flat surface (33°), the cos θ values for STO-823K and STO-923K are calculated to be 2.1 and 2.2, respectively. In both cases, cos θ is greater than 1.0, indicating that the water contact angle becomes 0°. Therefore, it is reasonable that the $SrTiO_3$ nanorod arrays in the present study exhibit excellent sustainabilities of hydrophilicity in dark places due to their rough surfaces. From a practical point of view, the sustainability of the surface wettability in a dark place is necessary for self-cleaning or antifogging applications.

Finally, to investigate the photocatalytic oxidative activities on $SrTiO_3$ nanorods, the wettability conversions on oleic acid applied surfaces were evaluated under UV illumination. Figure 8 shows the change in water contact angles under UV illumination. Immediately after applying oleic acid, both STO-823K and STO-923K surfaces are converted to highly hydrophobic states (with contact angles of 140°) due to the hydrophobic property of the oleic acid adsorbed on the surfaces. My previous study has revealed that the water contact angle on a polycrystalline $SrTiO_3$ film with a roughness factor (r) of 1.1 is about 70° when oleic acid is coated on the surface using methods similar to those in the present study.[12] The high hydrophobicities of $SrTiO_3$ nanorod arrays are also attributed to their rough surfaces. As previously mentioned, surface roughness enhances the hydrophobicity of a hydrophobic surface ($\theta > 90°$). When UV light is illuminated on the surface, both STO-823K and STO-923K films become super hydrophilic states with water contact angles below 3° because they both have photocatalytic activities. Inset

figures are photographs of water droplets on the surface of STO-923K. The water droplet was spread over the surface after 36 h of UV illumination. Although the detailed mechanism for the photoinduced hydrophilic reaction is still unclear, one plausible mechanism may be an increase in the hydroxyl groups on the photocatalyst surface, which proceeds in a different fashion than conventional photocatalytic oxidation reactions.[31] Several groups have reported that UV illumination on TiO_2 leads to an increase in adsorbed water molecules.[32] In addition to TiO_2, photoinduced hydrophilic conversions have been reported on various metal oxide semiconductors, such as ZnO,[33] WO_3,[34] SnO_2,[5c] and $InNbO_4$.[35] However, previous studies indicate that $SrTiO_3$ is inactive on photoinduced hydrophilic conversion, although it has a strong photocatalytic oxidative activity.[5c,12] Even if $SrTiO_3$ is inactive on photoinduced hydrophilicity, the surface of the $SrTiO_3$ nanorods becomes superhydrophilic by a oxidation reaction of the surface organic contaminants because their initial water contact angles are very low. Therefore, the superhydrophilic conversion in the present study is explained by the photocatalytic oxidation activity, and the superhydrophilicity of the $SrTiO_3$ nanorod arrays is due to the surface nanostructure. It is noted that the decreasing curves of water contact angles under UV illumination have two steps, i.e., water contact angles decreased gradually, then decreased sharply. This trend is due to the changes in coverage of oleic acid on the surfaces. My XPS analysis revealed that surface coverage of atomic carbon before UV illumination was 75%, and this coverage was not sharply decreased during the initial stage of UV illumination. Molecules of oleic acid are presumably adsorbed on the $SrTiO_3$ surface as a multilayered structure before UV illumination. During the initial stage of UV illumination, oleic acid molecules at interface layers are decomposed. After longer time illumination, water contact angles were sharply decreased, since the clean surface of $SrTiO_3$ was exposed by the decomposition of oleic acid. The surface coverage of atomic carbon was 26% after 40 h of UV illumination. The hydrophilicizing rate on STO-923K is faster than that on STO-823K because STO-923K has a higher crystallinity. The photocatalytic reaction involves photoexcitation and diffusion of the photogenerated charge carriers to a surface. Thus, the reaction rate depends on the mobility of the charge carriers. Therefore, in addition to the light absorption property, a high crystallinity is an important factor for an efficient photocatalytic reaction. Currently the photocatalytic activity of $SrTiO_3$ nanorods proceeds under UV illumination, but $SrTiO_3$ is considered to be one of the best candidates for visible light driven photocatalysts because the charge balance is easily controlled in the carrier-doping process. It is noteworthy that the starting material, titanate nanotubes, is an appropriate host material for the carrier-doping process due to its ion-exchangeability for various guest ions. Moreover, the present chemical process is one of the simplest methods to produce thin films of single-crystalline $SrTiO_3$ nanorods. This method may even be applicable to large-area processes. Furthermore, it has the potential as an economic route for industrial production of photocatalysis related applications. Besides photocatalytic applications, thin films in the present study have the potential for dielectric or optical devices.

Conclusions

Thin films of single-crystalline $SrTiO_3$ nanorods were successfully synthesized by a chemical process. Starting materials, titanate nanotubes, are ion-exchangeable, and Sr^{2+}-introduced titanate nanotubes were transferred to single-crystalline $SrTiO_3$ nanorods by annealing in air. These $SrTiO_3$ nanorods were oriented to the [110] direction of the perovskite phase and well adhered to the substrates. Although $SrTiO_3$ is known to be inactive in photoinduced hydrophilic reactions, $SrTiO_3$ nanorod arrays in the present study exhibited superhydrophilicity due to their surface nanostructures. These films had strong photocatalytic oxidative activities and excellent sustainability of the superhydrophilic states in dark conditions. The present fabrication method for thin films may even be applicable to a large-area process and has potential as an economic route for industrial production. Moreover, thin films of $SrTiO_3$ nanorods in the present study show promise for various industrial items, which have antifogging or self-cleaning properties.

Acknowledgment. I thank Mr. M. Oishi at AIST Electron Microscope Support Project for TEM measurement. This work was partly conducted in the AIST Nano-Processing Facility and was supported by "Nanotechnology Support Project" of the Ministry of Education, Culture, Sports, Science and Technology of Japan.

References and Notes

(1) Ohta, H.; Kim, S.-W.; Mune, Y.; Mizoguchi, T.; Nomura, K.; Ohta, S.; Nomura, T.; Nakanishi, Y.; Ikuhara, Y.; Hirano, M.; Hosono, H.; Koumoto, K. *Nat. Mater.* **2007**, *6*, 129.

(2) Millis, A. J. *Nature* **1998**, *392*, 147.

(3) Hill, N. A. *J. Phys. Chem. B* **2000**, *104*, 6694.

(4) Wessels, B. W. *Annu. Rev. Mater. Sci.* **1995**, *25*, 525.

(5) (a) Matsumura, M.; Hiramoto, M.; Tsubomura, H. *J. Electrochem. Soc.* **1983**, *130*, 326. (b) Wang, D.; Ye, J.; Kako, T.; Kimura, T. *J. Phys. Chem. B* **2006**, *110*, 15824. (c) Miyauchi, M.; Nakajima, A.; Watanabe, T.; Hashimoto, K. *Chem. Mater.* **2002**, *14*, 2812.

(6) Kato, H.; Kudo, A. *J. Phys. Chem. B* **2002**, *106*, 5029.

(7) Irie, H.; Murayama, Y.; Hashimoto, K. *J. Phys. Chem. C* **2007**, *111*, 1847.

(8) (a) Kasahara, A.; Nokumizu, K.; Takata, T.; Kondo, J. N.; Hara, M.; Kobayashi, H.; Domen, K. *J. Phys. Chem. B* **2003**, *107*, 791. (b) Miyauchi, M.; Takashio, M.; Tobimatsu, H. *Langmuir* **2004**, *20*, 232.

(9) Jiang, J.; Henry, L. L.; Gnanasekar, K. I.; Chen, C.; Meletis, E. I. *Nano Lett.* **2004**, *4*, 741.

(10) (a) Urban, J. J.; Yun, W. S.; Gu, Q.; Park, H. *J. Am. Chem. Soc.* **2002**, *124*, 1186. (b) Wang, G.; Sæterli, R.; Rørvik, P. M.; Helvoort, A. T. J.; Holmestad, R.; Grande, T.; Einarsrud, M-A. *J. Phys. Chem. C* **2007**, *19*, 2213.

(11) Mao, Y.; Banerjee, S.; Wong, S. S. *Chem. Commun.* **2003**, *3*, 408.

(12) Miyauchi, M.; Nakajima, A.; Fujishima, A.; Hashimoto, K.; Watanabe, T. *Chem. Mater.* **2000**, *12*, 3.

(13) (a) Miyauchi, M.; Tokudome, H. *J. Mater. Chem.* **2007**, *17*, 2095. (b) Miyauchi, M.; Tokudome, H.; Toda, Y.; Kamiya, T.; Hosono, H. *Appl. Phys. Lett.* **2006**, *89*, 043114.

(14) Chen, Q.; Zhou, W.; Du, G.; Peng, L. M. *Adv. Mater.* **2002**, *14*, 1208.

(15) (a) Ma, R.; Bando, Y.; Sasaki, T. *Chem. Phys. Lett.* **2003**, *380*, 577. (b) Ma, R.; Fukuda, K.; Sasaki, T.; Osada, M.; Bando, Y. *J. Phys. Chem. B* **2005**, *109*, 6210.

(16) Yang, J.; Jin, Z.; Wang, X.; Li, W.; Zhang, J.; Zhang, S.; Guo, X.; Zhang, Z. *Dalton Trans.* **2003**, *20*, 3898.

(17) Nakahira, A.; Kato, W.; Tamai, M.; Isshiki, T.; Nishio, K.; Aritani, H. *J. Mater. Sci.* **2004**, *39*, 4239.

(18) (a) Tokudome, H.; Miyauchi, M. *Angew. Chem., Int. Ed.* **2005**, *44*, 1974. (b) Tokudome, H.; Miyauchi, M. *Chem. Lett.* **2004**, *33*, 1108.

(19) Sun, X.; Li, Y. *Chem. Eur. J.* **2003**, *9*, 2229.

(20) Tokudome, H.; Miyauchi, M. *Chem. Commun.* **2004**, *8*, 958.

(21) Kubo, T.; Kato, W.; Yamasaki, Y.; Nakahira, A. *Key Eng. Mater.* **2006**, *317*−*318*, 247.

(22) Bavykin, D. V.; Friedrich, J. M.; Walsh, F. C. *Adv. Mater.* **2006**, *18*, 2807.

(23) Nian, J. N.; Teng, H. *J. Phys. Chem. B* **2006**, *110*, 4193.

(24) Bavykin, D. V.; Friedrich, J. M.; Lapkin, A. A.; Walsh, F. C. *Chem. Mater.* **2006**, *18*, 1124.

(25) Gateshki, M.; Yin, S.; Ren, Y.; Petkov, V. *Chem. Mater.* **2007**, *19*, 2512.

(26) Yin, S.; Akita, Y.; Komatsu, M.; Wang, J.; Tang, Q.; Sato, S. *J. Mater. Chem.* **2005**, *15*, 674.

(27) Bottin, F.; Finocchi, F.; Noguera, C. *Phys. Rev. B* **2003**, *68*, 035418.

(28) Lotnyk, A.; Senz, S.; Hesse, D. *J. Phys. Chem. C* **2007**, *111*, 6372.

(29) (a) Cardona, M. *Phys. Rev.* **1965**, *A651*, 140. (b) Soriano, L.; Abbate, M.; Fernandez, A.; Gonzalez-Elipe, A. R.; Sanz, J. M. *Surf. Interface Anal.* **1997**, *25*, 804. (c) Mo, S. D.; Ching, W. Y. *Phys. Rev. B* **1995**, *51*, 50.

(30) Wenzel, R. N. *J. Phys. Colloid Chem.* **1949**, *53*, 1466.

(31) Sakai, N.; Fujishima, A.; Watanabe, T.; Hashimoto, K. *J. Phys. Chem. B* **2003**, *107*, 1028−1035.

(32) (a) Nakamura, R.; Ueda, K.; Sato, S. *Langmuir* **2001**, *17*, 2298. (b) Nosaka, A. Y.; Kojima, E.; Fujiwara, T.; Yagi, H.; Akutsu, H.; Nosaka, Y. *J. Phys. Chem. B* **2003**, *107*, 12042. (c) Uosaki, K.; Yano, T.; Nihonyanagi, S. *J. Phys. Chem. B* **2004**, *108*, 19086.

(33) (a) Sun, R. D.; Nakajima, A.; Watanabe, T.; Hashimoto, K. *J. Phys. Chem. B* **2001**, *105*, 1984. (b) Miyauchi, M.; Shimai, A.; Tsuru, Y. *J. Phys. Chem. B* **2005**, *109*, 13307.

(34) Miyauchi, M.; Nakajima, A.; Hashimoto, K.; Watanabe, T. *Adv. Mater.* **2000**, *12*, 1923.

(35) Kako, T.; Ye, J. *Langmuir* **2007**, *23*, 1924.